2005-01-2410

Prediction of High Frequency Response Characteristics of Hydraulic Mounts

Song He and Rajendra Singh
Acoustics and Dynamics Laboratory
The Ohio State University

ABSTRACT

The major objectives of this study are to identify the source(s) of high frequency resonance(s), suggest a method to effectively estimate mount parameters and propose both linear and nonlinear models capable of predicting the high frequency characteristics. First, a lumped parameter linear model is derived and the resonances controlled by decoupler, fluid column and rubber element are examined. By using a simplified mechanical model, typical parameters are estimated from measured dynamic stiffness data. Estimations correlate well with experiments and provide quantitative evaluation of the physical parameters, some of which (such as the decoupler damping) are otherwise difficult to measure by using conventional experimental techniques. A nonlinear time domain model for a free decoupler mount is proposed to predict both the inertia track and decoupler resonances. Both nonlinear and linear models match well with high frequency measurements.

INTRODUCTION

MOTIVATION AND LITERATURE REVIEW

Hydraulic engine mounts are designed to provide superior amplitude-sensitive and spectrally-varying properties over the lower frequency regime (typically up to 50 Hz) [1]. However, at relatively higher frequencies (say from 50~300 Hz), the decoupler induced resonance could be dominant which would worsen their performance from the vibration isolation perspective. Singh *et al.* [1] developed linear time-invariant lumped parameter models for both free and fixed decoupler mounts. They suggested a multi degree of freedom (MDOF) fluid model. Ushijima *et al.* [2] suggested an analogy between mechanical and fluid elements in order to investigate the fluid resonance effect at higher frequencies. Lee *et al.* [3] modeled a hydraulic mount using the bond graph method, which was shown to be an efficient approach in developing the multi-disciplinary model equations. Colgate *et al.* [4] proposed two linear models for large amplitude and small amplitude excitations respectively though both models could be combined using piecewise functions. Geisberger *et al.* [5] examined the volume column effect within the decoupler regime and suggested a MDOF decoupler model as a remedy to the high frequency resonance. A “bell chamber” was also examined as an alternate way to suppress the decoupler resonance [6]. They proposed a decoupler model with exponential smoothening “stop” resistance to characterize the decoupler switching mechanism. Tiwari *et al.* [7-8] described a series of laboratory experiments to characterize various nonlinearities of fixed and free mounts. They also suggested a multi-staged switching model over the lower frequency regime (up to 50 Hz) to predict the transient behavior of the decoupler switching mechanism.

PROBLEM FORMULATION

Dominant inertial and standing wave effects may occur at higher frequencies (*f)* [11]. Further, prediction of higher frequency responses may demand a distributed parameter formulation along with a true nonlinear time domain model. However, simplifications can still be made depending on the frequency range of interest and the amplitude sensitivity of the particular mount design. Accordingly, key assumptions of this article are as follows. 1. The displacement excitation amplitude (X) is small (< 0.1 mm) over the higher frequency regime; this is due to the test machine limitations and low displacements found in vehicles at higher *f.* 2. For a free (or floating) decoupler hydraulic mount, the decoupler gap is assumed to remain open all the time and the governing system should be almost linear. 3. In this article, the hydraulic mount with a free decoupler is chosen although similar treatment could be extended to membrane type hydraulic mount. When an elastic membrane is used instead of a floating decoupler structure [2], the compliant membrane could accumulate the displaced fluid under small amplitude excitations. Thus, the inertia track is “decoupled” (or removed) from the system. 4. The driving point dynamic stiffness could be approximated by the measured cross point dynamic stiffness, especially at lower *f* [9]; this has been confirmed by the experimental work of Lee *et al.* [10]. The nonlinear lumped model suggested earlier by Adiguna *et al*. [8] is extended, in this article, to cover the

higher frequency regime. Predictions of the resulting linear MDOF model will be verified.

PROBLEM FORMULATION

PHYSICAL MODEL

Figure 1 shows the inner structure of a typical hydraulic mount (designated here as G). The rubber decoupler is placed between two inertia track plates with a small gap g_d . Also the working thickness around the decoupler center is 5.0 mm, which makes the decoupler plate relatively rigid (with low compliance C_d). These design features make the dynamic stiffness relatively insensitive to the displacement excitation amplitude *X* (peak to peak), as shown by the measured data of Figure 2.

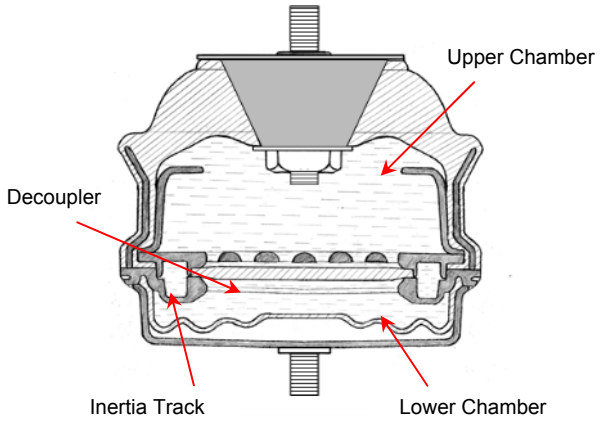

Fig.1 Schematic of free decoupler mount G.

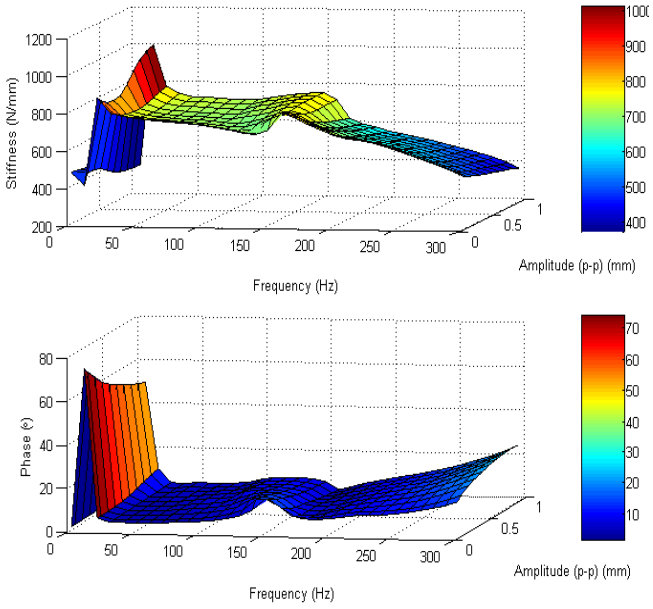

Fig. 2 Measured dynamic stiffness of mount G up to 300 Hz.

MDOF FLUID SYSTEM MODEL

We develop a MDOF fluid model of a free decoupler mount by considering several control volumes as shown in Figure 3. The Voight visco-elastic formulation is used to characterize the rubber element in terms of dynamic stiffness k_r and damping b_r that are weakly dependent on *f* and *X*.

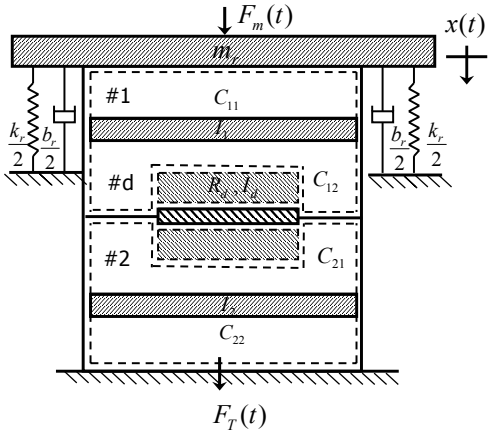

Fig. 3 Schematic of the lumped fluid model.

The top chamber control volume (#1) is lumped into a fluid mass $m_1 = \rho V_1$ or inertance $I_1 = m_1 / A_r^2$ with compliances C_{11} and C_{12} [1]. C_{11} incorporates the series connection of the compliances of the liquid and the rubber container, which is approximated as a solid cylinder fixed at all surfaces except the face contacting the fluid. C_{12} incorporates a series connection of liquid and decoupler compliance C_d. Note that additional compliance induced by entrapped air is not included in equations (1-3), where l_r is the rubber thickness, ν is the Poisson's ratio, E_r is the Young's modulus of rubber material and A_r is the effective piston area.

$$C_{11} \approx \frac{A_r l_r \left(1 - 3\nu^2 - 2\nu^3\right)}{\left(1 - \nu^2\right) E_r} \tag{1a}$$

$$C_{12} \approx \frac{V_1}{2B_l} + C_d \approx C_d \tag{1b}$$

Similarly, the lower chamber fluid volume (#2) is lumped into a fluid mass $m_2 = \rho V_2$ or inertance $I_2 = m_2 / A_r^2$. The compliances C_{11} and C_{12} can be estimated by approximating the rubber bellow as a hemispherical membrane [1].

$$C_{21} = C_{22} \approx \frac{1}{2} C_2 \approx \frac{\pi d_2^4}{32 t_2 E_r} \tag{2}$$

The convoluted rubber bellow of Figure 1 is designed as an accumulator with large compliance so that the lower chamber (absolute) pressure can be approximated by the atmosphere pressure. Also the lower chamber

volume (42.6 ml for mount G) is usually small compared with the upper chamber volume (155.0 ml for mount G), which implies the resonance frequency of lower chamber fluid column is much higher that of the upper chamber. Consequently, further simplification is possible to treat the lower chamber fluid spring as an air spring. One inertial lump is chosen to represent the decoupler as well as the fluid inertia within the perturbation region as shown in Figure 3, where A_d is the decoupler working area. The viscous resistance induced by fluid flow at the decoupler perimeter is characterized by R_d.

SIMPLIFIED MECHANICAL MODEL

Since the inertia track is assumed to be "decoupled" for small X excitations at higher f, only x(t), x_1(t), x_d(t), and x_2(t) are considered to derive the governing equations of the 4DOF system. Further, a force excitation F(t) is assumed here that would produce displacement response x(t). Application of the momentum equations yields:

$$F(t) - k_r x - b_r \dot{x}(t) - A_r p_{11}(t) = m_r \ddot{x}(t) \quad (3a)$$

$$\left(p_{11}(t) - p_{12}(t)\right) A_r = m_1 \ddot{x}_1(t) \quad (3b)$$

$$p_{12}(t) - p_{21}(t)_r = I_d \dot{q}_d(t) + R_d q_d(t) \quad (3c)$$

$$p_{21}(t) - p_{22}(t)_r = m_2 \ddot{x}_2(t) \quad (3d)$$

Application of the continuity equations yields:

$$A_r \left[\dot{x}(t) - \dot{x}_1(t)\right] = C_{11} \dot{p}_{11}(t) \quad (4a)$$

$$A_r \dot{x}_1(t) - q_d(t) = C_{12} \dot{p}_{12}(t) \quad (4b)$$

$$q_d(t) - A_r \dot{x}_2(t) = C_{21} \dot{p}_{21}(t) \quad (4c)$$

$$A_r \dot{x}_2(t) = C_{22} \dot{p}_{22}(t) \quad (4d)$$

Define effective stiffness, damping and mass terms as:

$$k_{11} = \frac{A_r^2}{C_{11}}, \quad k_{12} = \frac{A_r^2}{C_{12}}, \quad k_{21} = \frac{A_r^2}{C_{21}}, \quad k_{22} = \frac{A_r^2}{C_{22}}$$

$$\dot{x}_d(t) = \frac{q_d(t)}{A_d}, \quad m_d = I_d A_r^2 = \frac{A_r^2}{A_d^2} m_{d0}$$

$$b_d = R_d A_r^2 = \frac{A_r^2}{A_d^2} b_{d0} \quad (5a\text{-}g)$$

Combining equations (3-4) using the effective parameters in mechanical units and eliminate internal variables p_{11}, p_{12}, p_{21} and p_{22}:

$$m_r \ddot{x}(t) + b_r \dot{x}(t) + k_r x(t) + k_{11}\left[x(t) - x_1(t)\right] = F(t)$$

$$m_1 \ddot{x}_1(t) + k_{11}\left[x_1(t) - x(t)\right] + k_{12}\left[x_1(t) - x_d(t)\right] = 0$$

$$m_d \ddot{x}_d(t) + b_d \dot{x}_d(t) + k_{12}\left[x_d(t) - x_1(t)\right] + k_{21}\left[x_d(t) - x_2(t)\right] = 0$$

$$m_2 \ddot{x}_2(t) + k_{21}\left[x_2(t) - x_d(t)\right] + k_{22} x_2(t) = 0 \quad (6a\text{-}d)$$

Equations (6a-d) correspond to the governing equations of m_r, m_1, m_d and m_2 in the simplified 4DOF mechanical model of Figure 4.

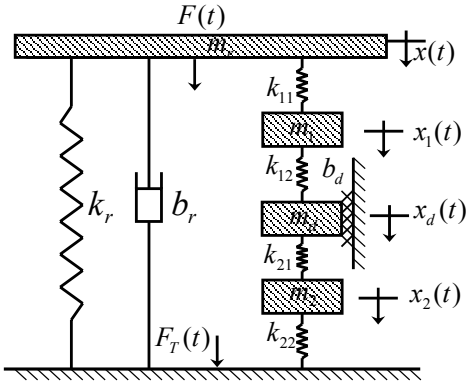

Fig. 4 A simplified mechanical model with 4DOF proposed to describe the higher frequency dynamics.

Rewrite (13-16) in matrix form as:

$$M\ddot{X} + C\dot{X} + KX = W \quad (7)$$

$$M = \begin{bmatrix} m_r & 0 & 0 & 0 \\ 0 & m_1 & 0 & 0 \\ 0 & 0 & m_d & 0 \\ 0 & 0 & 0 & m_2 \end{bmatrix}, C = \begin{bmatrix} b_r & 0 & 0 & 0 \\ 0 & 0 & 0 & 0 \\ 0 & 0 & b_d & 0 \\ 0 & 0 & 0 & 0 \end{bmatrix}, X = \begin{bmatrix} x \\ x_1 \\ x_d \\ x_2 \end{bmatrix}$$

$$K = \begin{bmatrix} k_r + k_{11} & -k_{11} & 0 & 0 \\ -k_{11} & k_{11} + k_{12} & -k_{12} & 0 \\ 0 & -k_{32} & k_{12} + k_{21} & -k_{21} \\ 0 & 0 & -k_{21} & k_{21} + k_{22} \end{bmatrix}, W = \begin{bmatrix} F \\ 0 \\ 0 \\ 0 \end{bmatrix}$$

Modal analysis is conducted by using stiffness (K) and mass (M) matrices and by finding the eigenvalues of $M^{-1}K$. Further, the dynamic compliance frequency response function (inverse of the dynamic stiffness) is derived (in matrix form) as follows where ω is the frequency in rad/s:

$$\frac{X}{F} = \left(-M\omega^2 + jC\omega + K\right)^{-1} \begin{bmatrix} 1 & 0 & 0 & 0 \end{bmatrix}^T \quad (8)$$

Make the following assumptions for the lower chamber: $k_2 \approx 0$ (air spring) and $m_1 >> m_2$. Thus, a simplified 3 DOF system is obtained and shown in Figure 5.

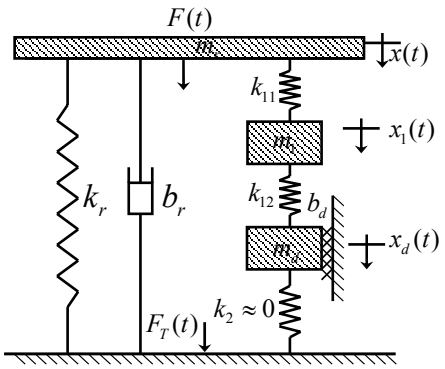

Fig. 5 Reduced order mechanical model (3DOF) over the higher frequencies.

Table 1 Parameters of mount G

k_r	440 N/mm	V_1	155 cm^3
b_r	300 N-s/m	V_2	42.6 cm^3
m_r	0.12 kg	ρ	1059 kg/m^2
k_1	376 N/mm	m_1	0.164 kg
k_{11}	188 N/mm	m_2	0.045 kg
k_{12}	188 N/mm	A_p	37 cm^2
k_2	0 N/mm	A_d	16 cm^2
b_{d0}	9.7 N-s/m	m_{d0}	0.012 kg

Several estimation procedures are employed to obtain the mount parameters as listed in Table 1: (i) Fluid masses m_1 and m_2 of upper and lower chambers are calculated from measured chamber volumes V_1 and V_2; (ii) Rubber element mass m_r, decoupler mass m_{d0} and decoupler area A_d are measured given the take-apart mount dimensions; (iii) Effective piston area A_r is estimated from measured mount cross-sectional area by assuming a 20% error bound; (iv) Assume that $k_{11} = k_{12} = k_1/2$, where the upper chamber fluid stiffness $k_1 = A_r^2/(C_{11}+C_{12})$ is estimated from inertia track resonance frequency (16 Hz) or by curve-fitting the dynamic stiffness over the lower *f* (up to 50 Hz) using the mechanical model. Refer to He and Singh [12] for details. Further, b_{d0} is estimated from the damping value at resonance.

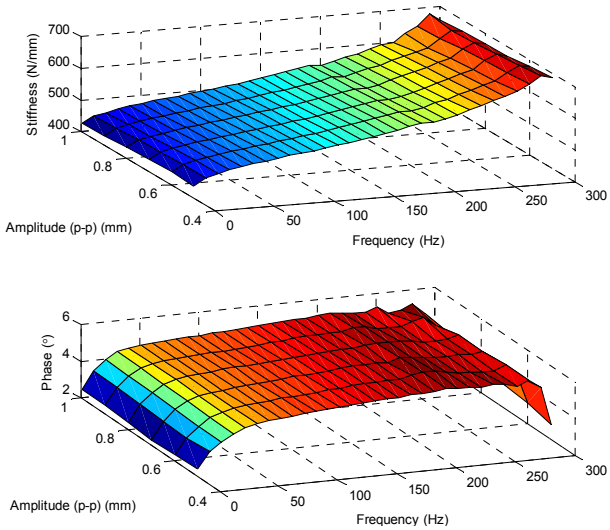

Fig. 6 Measured dynamic stiffness of the rubber element of mount G up to 300 Hz, given *X* = 0.5~1 mm (p-p).

The rubber stiffness k_r and damping b_r are approximated using the Voight visco-elastic model from measured dynamic stiffness of the cup-shaped primary rubber element with fluid drained out of the hydraulic mount (Figure 6). Constant values are assigned since the measured spectra depend do not vary much with excitation amplitude *X*. Note that only dynamic stiffness tests (other than conventional mass and geometric measurements) are required, which could be easily performed by commercial elastomer test machines [9].

The dynamic stiffness of the 3DOF mechanical system ($k_2 \approx 0$) is plotted in Figure 7 using equation (18). Prediction correlates well with measurements (re-plotted in the 2D form in Figure 8), especially in terms of the high frequency resonance around 150 Hz. Note that the low frequency resonance induced by the inertia track can not be predicted by this model.

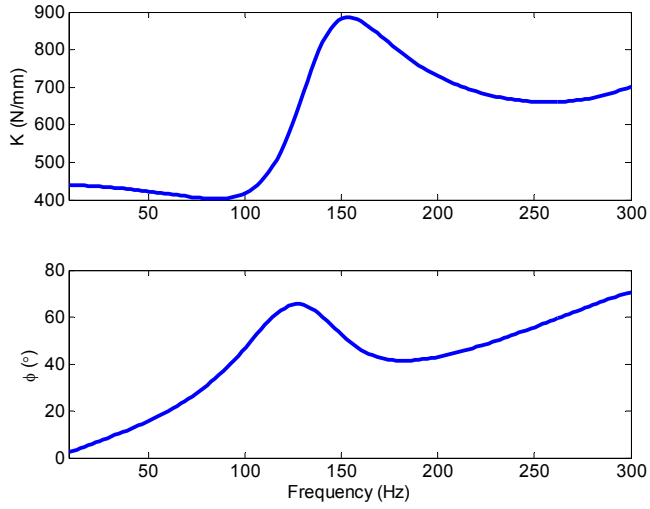

Fig. 7 Predicted dynamic stiffness of mount G using linear 3DOF model of Fig. 4.

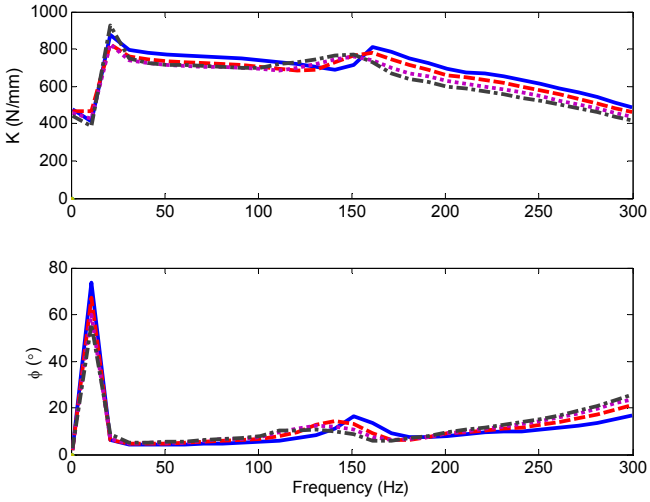

Fig. 8 Measured dynamic stiffness of mount G up to 300 Hz. Key: — X = 0.05 mm, - - - X = 0.2 mm, ····· X = 0.4 mm, -·-·- X = 0.6 mm.

Displacement mode shapes of the 3DOF mechanical model (of Figure 5) are plotted in Figure 9 corresponding to three natural frequencies. The lower chamber fluid mass m_2 has zero motion due to the $k_2 \approx 0$ assumption. For mode I at 116 Hz, all masses vibrate in phase. Observe that the decoupler mass m_d has the maximum amplitude, which implies that mode I is dictated by the decoupler resonance. Similarly, the decoupler motion also dominates mode II at 323 Hz. However, now m_d is out of phase with other masses m_r and m_d . Further, the natural frequencies of modes II and III are close to each other, thus a coupling may exist between these two modes. Also note that for mode III, m_r has the maximum amplitude and m_1 vibrates out of phase relative to other masses. Consequently, it is implied that mode III is governed by rubber and upper chamber fluid column resonances.

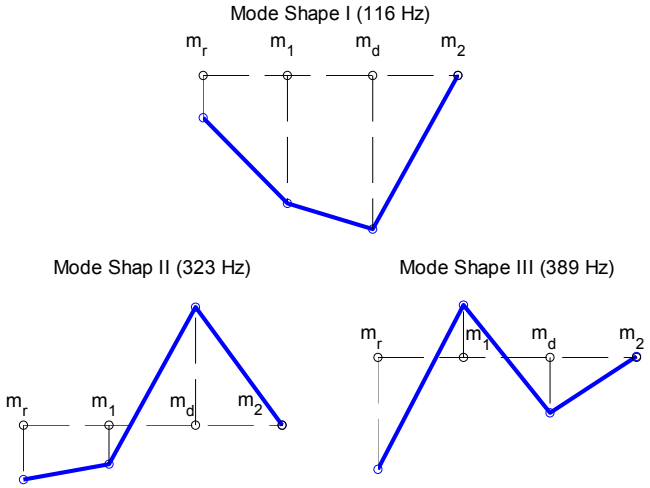

Fig. 9 Displacement mode shapes of the 3DOF mechanical model of Fig. 5.

RESONANCE TUNING USING THE MDOF MODEL

Modal study of the MDOF mechanical model shows that the decoupler resonance dominates the high frequency resonance (around 150 Hz). This mode is also influenced by rubber and fluid column inertias. This guideline together with the MDOF model can be easily implemented to examine some high frequency resonance tuning concepts such as “bell plate” and “MDOF decoupler” [6].

Resonance Tuning Using a Bell Plate

Geisberger *et a.l* [6] suggested that the tuning flexibility can be enhanced by adding a “bell plate” to the upper chamber (mount Q) at the excitation point. Note that mount Q of Figure 10 is very similar to mount G of Figure 1 in terms of the inner structure. The additional DOF associated with the bell fluid inertia was tuned to alleviate the decoupler resonance as shown in Figure 11 [6].

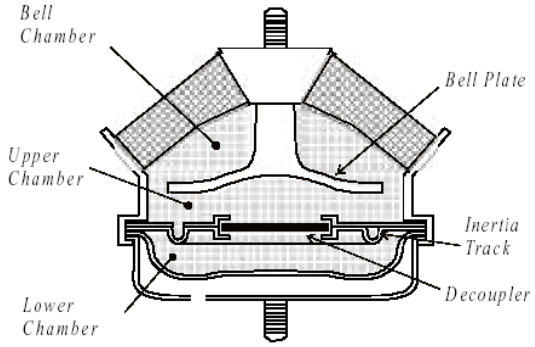

Fig.10 Cross section of mount Q with a bell plate in the upper chamber; extracted from Geisberger *et al.* [6].

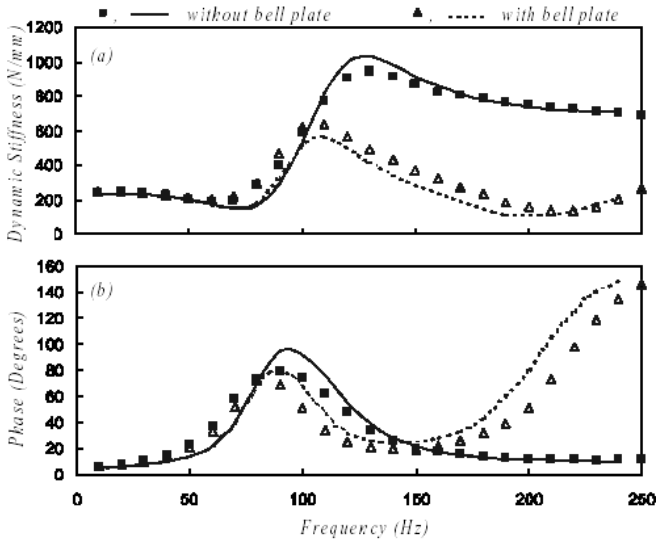

Fig. 11 Dynamic stiffness of mount Q with X = 0.1mm. Results are extracted from Geisberger *et al.* [6]. Key: “■, — ” without and “▲, - - -” with bell plate structure.

The bell plate separates the upper chamber into two parts and introduces a fixed boundary condition inside the chamber. Since the rubber element is much more compliant than the rigid bell plate, fluid inside the bell chamber is assumed to vibrate in phase with m_r over the higher frequency range of interest (50~350 Hz), resulting in an effective rubber mass with increased inertia $m_{re} > m_r$. Likewise, more fluid is assumed to be in the perturbation region around the decoupler ($m_{de} > m_d$) due to the rigid plate effect. Consequently, less fluid remains below the bell plate corresponding to an effective fluid column mass $m_{1e} < m_1$. Use the 3DOF mechanical model to examine the bell chamber effect by assuming $m_{re} = m_r + 0.4m_1$, $m_{1e} = 0.4m_1$ and $m_{d1} = m_d + 0.2m_1$. Simulated dynamic stiffness is found and plotted in Figure 12.

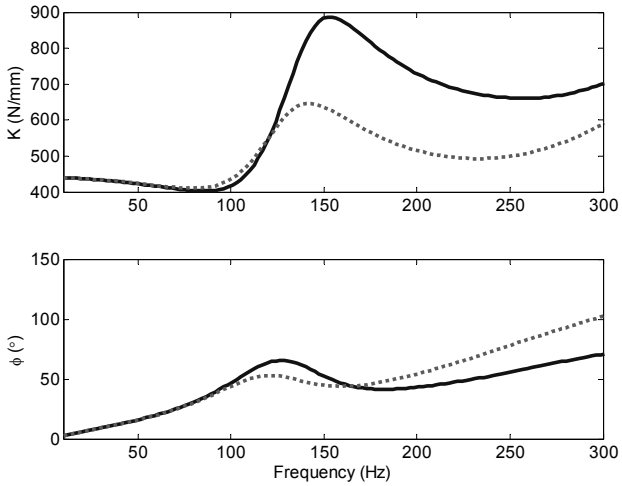

Fig. 12 Predicted dynamic stiffness of mount G using 3DOF model. Key: "— " original (without bell plate), " · · ·" with a bell plate. Corresponding experimental results are in Fig. 11.

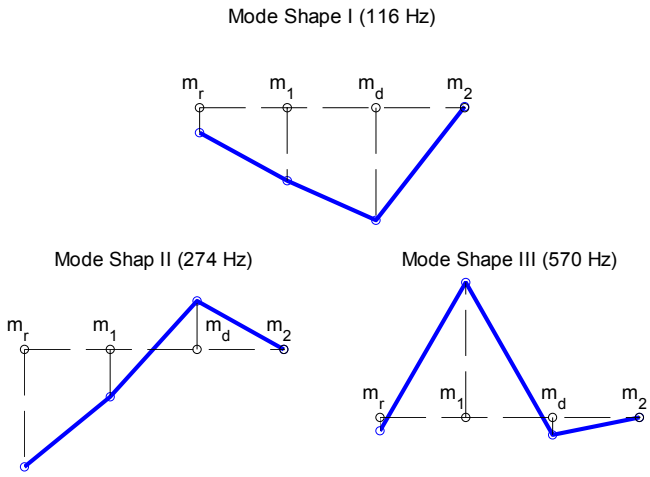

Fig. 13 Displacement mode shapes of the 3DOF model considering the effect of a bell plate in the upper chamber (a design suggested by Geisberger *et al.* [6]).

Predicted dynamic stiffness of Figure 12, along with changes introduced by the bell chamber, show the same feature as reported in experimental data of Figure 11 [6]. The high frequency resonance tuning effect may be further explained by a comparative study on the displacement mode shapes between Figure 9 (the original system) and Figure 13 (the modified system with a bell chamber). Mode I at 116 Hz is still dictated by decoupler resonance and it remains almost unaffected by the bell chamber. Natural frequencies of mode II and III are separated from 323 to 389 Hz and from 274 to 570 Hz respectively, which implies that the coupling effect between two modes is significantly reduced. Mode II is dominated by the rubber element instead of decoupler mass, with an introduction of the bell chamber. Mode III is predominately governed by the fluid column resonance; since this natural frequency has been shifted to a much higher frequency (570 Hz) compared with the frequency regime of interest, thus its influence is minimized. Overall, the peak value in the dynamic stiffness around 150 Hz is found to be lower, followed by a rapid increase in the loss angle. This implies the presence of anti-resonance. Further, parametric studies could be conducted based on the MDOF mechanical model to allocate an "optimized" fluid volume within the bell chamber for most desirable tuning.

Resonance Tuning Using the MDOF Decoupler

Similar high frequency tuning effects could be achieved by introducing additional DOFs via a "MDOF decoupler" as suggested by Geisberger *et al.* [5]. The decoupler is fixed at the perimeter and an additional compliance is introduced the center as shown in Figure 14. This concept would create two coupled flow paths through the decoupler [5]. A modified mechanical model with additional DOFs corresponding to the lumped fluid masses of Figure 14 could be developed.

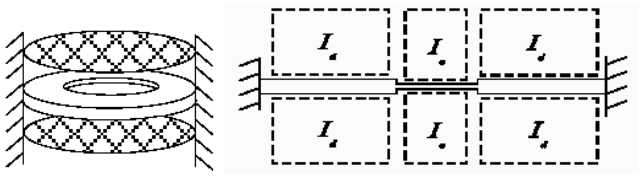

Fig 14. (a) MDOF decoupler concept; (b) Lumped fluid model around decoupler, extracted from Geisberger *et al* [5].

ESTIMATION OF MOUNT PARAMETERS

SIMPLIFIED 2DOF MECHANICAL MODEL

In order to minimize the experimental work required in creating a high frequency model, it is desirable to estimate the mount parameters directly from measured dynamic stiffness data using a simplified mechanical model. When the resonance frequency of the fluid mass

m_1 (389 Hz for mount G) is higher than the frequency regime of interest (typically 50 to 300 Hz), the MDOF system can be further simplified into a 2DOF model by ignoring the fluid column inertia ($m_1 \approx 0$) as shown in Figure 15. Note that estimated (effective, represented by subscript *e*) parameters might be different from the values of Table 1 due to alternate modeling strategies. Nevertheless, either model could be consistently implemented to characterize various hydraulic mounts for a comparative study.

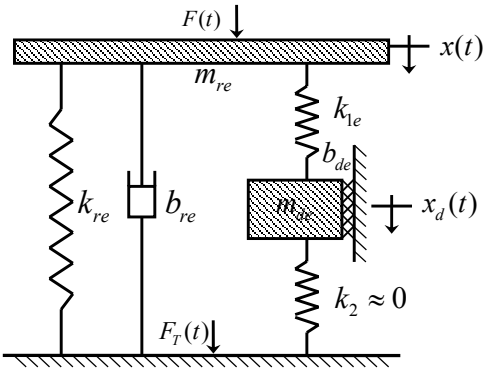

Fig. 15 Simplified 2DOF high frequency mechanical model.

Rewrite the governing equations (3-4) by ignoring the fluid masses m_1 and m_2 and assuming $k_{1e} = k_{11} + k_{12} >> k_{2e} \approx 0$ (or $p_2(t) \approx 0$) to yield the following:

$$F(t) = k_{re}x(t) + b_{re}\dot{x}(t) + A_p p_1(t) + m_{re}\ddot{x}(t) \quad (9a)$$

$$-q_d(t) = C_1\dot{p}_1 - A_p\dot{x}(t) \quad (9b)$$

$$m_{d0}\ddot{x}_d(t) + b_{d0}\dot{x}_d(t) = A_d p_1(t) \quad (9c)$$

$$q_d(t) = A_d\dot{x}_d(t) \quad (9d)$$

A 4th/2nd order linear dynamic stiffness transfer function in the Laplace (*s*) domain is obtained as:

$$K_{42m}(s) = m_{re}s^2 + b_{re}s + k_{1e} + k_{re} - \frac{k_{1e}^2}{m_{de}s^2 + b_{de}s + k_{1e}} \quad (10a)$$

Curve-fit the measured dynamic stiffness over the higher frequency regime using the following 4th/2nd order transfer function:

$$K_{42}(s) = \frac{n_4 s^4 + n_3 s^3 + n_2 s^2 + n_1 s + n_0}{d_2 s^2 + d_1 s + d_0 s} \quad (10b)$$

Comparison of equations (10a-b) shows that coefficients d_2, d_1 and d_0 are proportional to m_{de}, b_{de} and k_{1e} respectively. Assuming an empirical scaling factor θ_0, estimate the mechanical system parameters as follows where γ is defined as an adjustment ratio that varies with *X*. The γ ratio is used to fine tune the factor θ_0 to achieve best possible curve-fit results.

$$k_{re} = \frac{n_0}{d_0}, \quad m_{re} = \frac{n_4}{d_2}, \quad b_{re} = \frac{d_2 n_3 - n_4 d_1}{d_2^2}$$

$$\theta_0 = d_1 / \left(\frac{n_1}{d_0} - \frac{n_0 d_1}{d_0^2} - b_r \right),$$

$$k_{1e} = \frac{d_0}{\gamma\,\theta_0}, \quad b_{de} = \frac{d_1}{\gamma\,\theta_0}, \quad m_{de} = \frac{d_2}{\gamma\,\theta_0} \quad (11a\text{-}f)$$

Figure 16 compares measured, curve-fitted and predicted dynamic stiffness of mount G at *X* = 0.1 mm over the higher frequency regime. It is shown that predictions match measurements well. Parameters estimated using (11) are listed in Table 2.

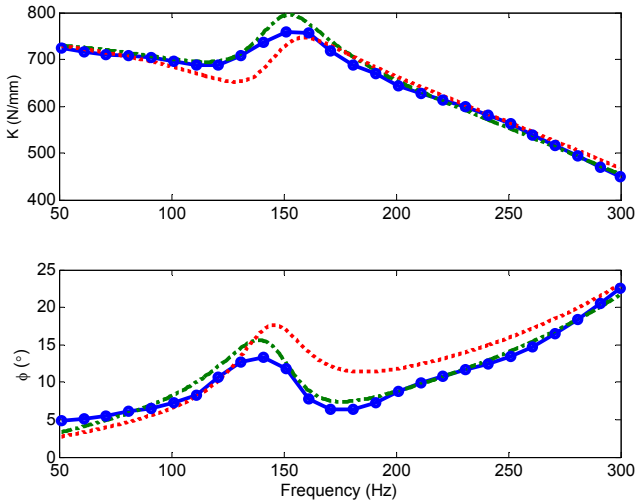

Fig. 16 Dynamic stiffness of mount G with *X* = 0.1 mm. Key: measurement, 4th/2nd curve-fit, predicted using the 4th/2nd mechanical model.

Table 2. Mechanical system parameters estimated for mount G using the model of Fig. 15 and measured data of Fig. 16.

Parameters	X (mm) p-p				
Symbols	0.1	0.3	0.5	0.7	0.9
k_{1e} [N/mm]	42.6	37.9	23.6	17.0	13.2
k_{re} [N/mm]	779	741	728	735	735
b_{re} [Nm/s]	82.9	96.4	104	104	104
b_{de} [Nm/s]	10.5	10.5	8	5.3	4.1
m_{de} [g]	46	44	29	21	16
m_{re} [g]	102	99.8	101	106	106
γ	2.0	3.5	5.0	7.0	9.0

Several interesting conclusions can be drawn by examining the effective parameters of Table 2. First, the estimated value of m_{re} is comparable to measured value of m_r as well as m_{de}. This confirms the necessity of including m_r in the simplified 2DOF model. Second, estimated value of k_{re} is as high as 730 N/mm, which implies the rubber is stiffer at higher frequency. Measurements of the rubber element in Figure 6 confirm the stiffening characteristics as K increases from 420 N/mm at 10 Hz steadily to roughly 700 N/mm at 300 Hz. Note that the estimated values of k_{1e} and k_{re} are different from those of k_1 and k_r in Table 1. It is because that k_{1e} and k_{re} are estimated from measured spectra, part of which (lower than 120 Hz) is significantly influenced by the inertia track resonance. Nevertheless, an interesting empirical relationship is also observed: $k_1 + k_r$ value of Table 1 is essentially the same as estimated $k_{1e} + k_{re}$ value of Table 2. This implies the two different modeling strategies (4DOF vs. 2DOF) are interrelated. Third, the b_{re} value remains consistent and b_{de} is significantly smaller than b_{ie} [9]. This would ensure lower damping and stiffness in the high frequency regime; such properties are indeed desirable from the vibration isolation perspective. Fourth, when X is increased, m_{de} and b_{de} tend to decrease. This is because more fluid would flow through the inertia track under a higher X since less fluid remains around the decoupler in the top chamber. This also explains the "flip" characteristics of the higher frequency resonance near 150 Hz as shown in Figure 2. Finally, the adjustment ratio γ is somewhat proportional to X. Therefore, it could be used to quantify the amplitude dependence of the natural frequency.

VERIFICATION OF LINEAR MODLES USING A NONLINEAR FORMULATION

COMPARATIVE STUDY OF ALTERNATE NONLINEAR MODELS

True nonlinear models (solved in time domain) would be required to precisely predict the decoupler dominated resonance in the higher frequency regime with the additional benefit of simultaneously capturing the inertia track induced resonance in the low frequency regime. The key to such a broadband model is to incorporate the nonlinear decoupler switching mechanism, which is highly sensitive to the excitation amplitude X and transient internal flow. Two such nonlinear models have been suggested by Adiguna *et al.* [8] (designated here as Model I) and Geisberger *et al.* [12] (designated here as Model II). Model I employs a multi-stage decoupler switching model which was originally proposed to predict the mount dynamics in the low frequency regime up to 50 Hz. Its application is, however, extended to the high frequency regime up to 300 Hz in our study. Model II utilizes a smoothening function to simulate changes in the effective decoupler resistance during the switching transition. A comparative study is conducted to evaluate the alternate modeling techniques and verify the high frequency resonance prediction of our linear model.

Model I: Based on the lumped fluid model of Figure 17, governing equations are written using the momentum and continuity equations as follows:

$$q_i(t) + q_d(t) = A_p\dot{x}(t) - C_1(p_1)\dot{p}_1(t) \quad (11a)$$

$$-q_i(t) - q_d(t) = C_2(p_2)\dot{p}_2(t) \quad (11b)$$

$$F_T(t) = b_r\dot{x}(t) + k_r x(t) + A_p\left[\overline{p} - p_1(t)\right] \quad (11c)$$

$$I_i\dot{q}_i(t) + R_i(\Delta p_{12}, q_i)q_i(t) = p_2(t) - p_1(t) \quad (11d)$$

$$m_d\ddot{x}_d(t) + b_d\dot{x}_d(t) = A_d\left[p_2(t) - p_1(t)\right] \quad (11e)$$

$$q_d = A_d\dot{x}_d \quad (15a\text{-}f)$$

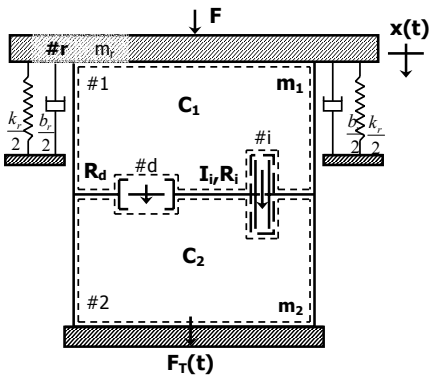

Fig. 17 Model I: Nonlinear fluid model of a free decoupler mount [7, 8].

Here, $C_1(p_1)$, $C_2(p_2)$ and $R_i(\Delta p_{12}, q_i)$ are nonlinear functions that are experimentally determined [7,8]. The decoupler switching mechanism is simulated based on the instantaneous decoupler position x_d and the direction of pressure difference $p_2(t) - p_1(t)$ between two chambers. When the decoupler closes, all fluid is assumed to flow through the inertia track with leakage flow neglected. Refer to Adiguna *et al.* [8] for details.

Model II: The governing equations are given below, with the signs of $p_1(t)$ and $p_2(t)$ defined in opposite directions [12].

$$C_1\dot{p}_1(t) = A_p\dot{x}(t) - q_i(t) - q_d(t)$$

$$C_2\dot{p}_2(t) = q_i(t) + q_d(t)$$

$$F_T(t) = b_r\dot{x}(t) + k_r x(t) + \left(A_p - A_d\right)\left[p_1(t) - p_2(t)\right] + A_p p_2(t) + A_d\left(R_d + R_d'\left|q_d(t)\right|\right)q_d(t)$$

$$p_1(t) - p_2(t) = I_d\dot{q}_d(t) + \left(R_d + R_d'\left|q_d(t)\right| + R_{add}\right)q_d(t)$$

$$p_1(t) - p_2(t) = I_i\dot{q}_i(t) + \left(R_i + R_i'\left|q_i(t)\right|\right)q_i(t)$$

(12a-e)

A smoothening function $R_{add} = R_0 e^{(x_d / X_0)\arctan(q_d / q_0)}$ is employed to stop the decoupler flow q_d by introducing significant resistance to R_d when the decoupler bottoms out as shown in Figure 18. Refer to Geisberger *et al*. [12] for details.

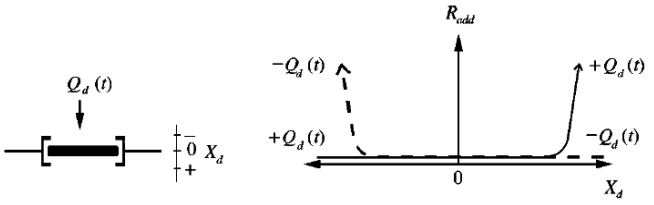

Fig. 18 Model II with a smoothening function [12].

Observe both models share the same governing equations for upper and lower chamber control volumes. Also, empirical data of [12] show that the turbulent resistance terms are negligible for both decoupler and inertia track dynamics. We employ the parameters of Table 3 to evaluate both nonlinear models.

Table 3 Simulation parameters, extracted from [12]

k_r	225e3 N/m	m_d	0.0327 kg
b_r	300 N-s/m	R_i	1.05e8 kg/s-m^4
C_1	3.0e-11 m^5/N	R_d	1.17e7 kg/s-m^4
C_2	2.6e-9 m^5/N	A_p	25 cm^2
I_i	3.38e6 kg/m^4	A_d	6.6 cm^2
I_d	7.5e4 kg/m4	l_d	1.06e-3 m

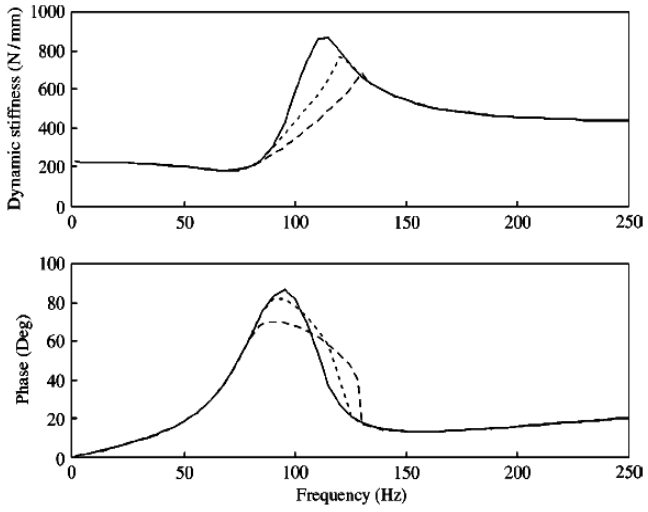

Fig. 19 Predicted dynamic stiffness over the higher frequency regime using Model II [12]. Key: — X = 0.05 mm, ····· X = 0.075 mm; - - - X = 0.1 mm.

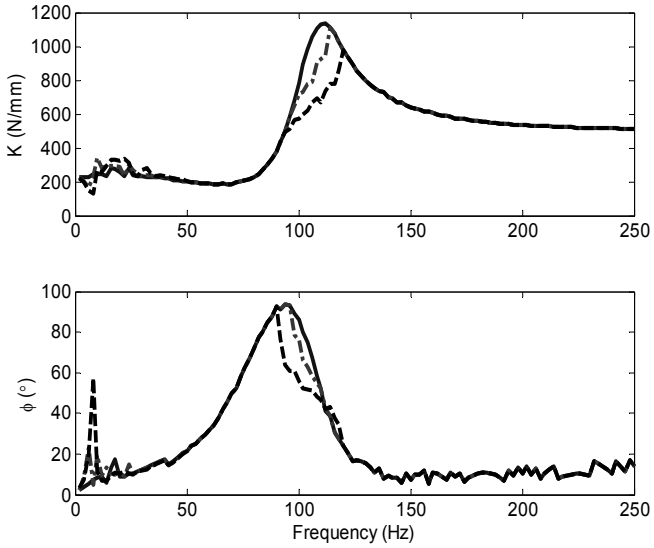

Fig. 20 Predicted dynamic stiffness over the higher frequency regime using Model I [7,8]. Key: — X = 0.05 mm, -·-·- X = 0.075 mm; - - - X = 0.1 mm

The steady state responses under sinusoidal excitations are numerically simulated in time domain and results are transformed into frequency domain to obtain the dynamic stiffness as shown in Figures 19 and 20. Simulation results of two nonlinear models correlate well for the decoupler induced resonance in terms of stiffness amplitude, loss angle and resonance frequency around 100 Hz. Consequently, both models are indeed capable of predicting the high frequency resonance well although different modeling techniques are applied.

VERIFICATION OF THE MDOF LINEAR MODEL

Nonlinear model I is used to predict the dynamic stiffness for mount G as shown in Figure 21. Baseline values of Table 1 are converted into the fluid system units and the inertia track related parameters are estimated from the low frequency resonance [9]. The decoupler inertia being used is several times larger than the measured value of Table 1 in order to tune the decoupler resonance frequency. This implies the effective decoupler inertia also includes the fluid in the region surrounding the decoupler. Predicted results of Figure 21 match well with measurements of Figure 8 in terms of both the inertia track and decoupler resonances over the entire frequency range. Observe that the dynamic stiffness depends weakly on the excitation amplitude X due to the small decoupler gap distance ($g_d \approx 0.3$ mm). This narrow gap may also lead to significant squeeze film effect [8], which would bring higher damping to the decoupler resonance and effectively suppresses the resonance amplitude. The over-estimation of peak stiffness in the low frequency range suggests other mechanisms including turbulent flow, which could bring additional damping to the inertia track resonance.

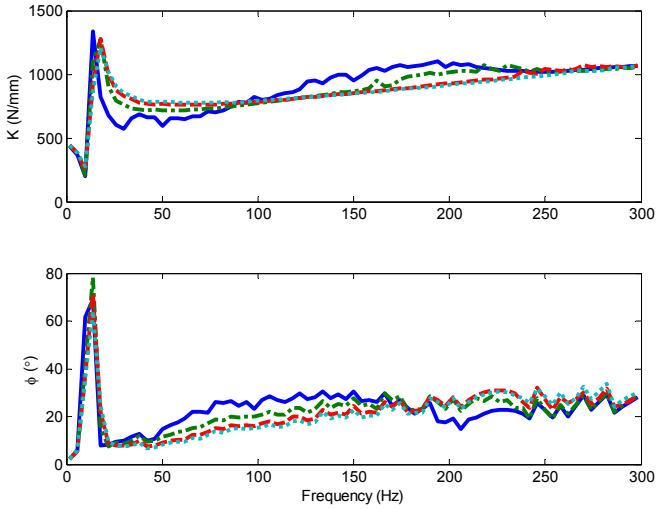

Fig. 21 Predicted dynamic stiffness of mount G using nonlinear model I. Key: — X = 0.1 mm, - - - X = 0.2 mm, ····· X = 0.4 mm, -·-·- X = 0.6 mm.

Parametric studies are conducted using the parameters of mount Q, which exhibits a more dominant decoupler resonance when compared with that of mount G. The undamped decoupler natural frequency (in rad/s) is predicted as follows using a simplified linear model:

$$\omega_n = \sqrt{\frac{(k_1 + k_2)\sigma^2}{m_d}} = \sqrt{\frac{A_d^2}{m_d}\left(\frac{1}{C_1} + \frac{1}{C_2}\right)} \qquad (13)$$

The natural frequencies for different decoupler inertia values are predicted using both the nonlinear (Model I) and linear models and compared in Table 4. Predictions match well and show the same trends. The nonlinear model yields more accurate predictions over the entire frequency range but it demands significant modeling and calculation efforts. On the other hand, the linear model could be easily implemented as an efficient tool for altering decoupler resonance. However, it can not predict any amplitude dependence.

Table 4 Comparison between resonance frequencies predicted by nonlinear and linear models

Freq. [Hz]	ω_{n1}	ω_{n2}	ω_{n3}	ω_{n4}	ω_{n5}
Nonlinear model (I)	42	84	112	158	>200
Linear model	34	76	107	151	338

CONCLUSION

A simplified MDOF mechanical model is formulated to predict the high frequency decoupler resonance. The effects of fluid column and rubber element are also examined, which could lead to several resonance tuning concepts such as the introduction of “bell chamber” [12]. Typical system parameters are estimated from measured decoupler resonance spectra using a simplified mechanical model, thus the experimental work is minimized. Two nonlinear models with alternate decoupler modeling techniques are comparatively evaluated. Predictions from one of the nonlinear models correlate well with that of the linear model as well as with measurements. Finally, both nonlinear models (I and II) are employed to successfully predict the low frequency behavior using the parameters that were extracted from [12]. Figures 22 and 23 compare the predicted results, which correlate well. These models lead to broadband nonlinear formulations which are beyond the scope of this article but may be found in [7, 12].

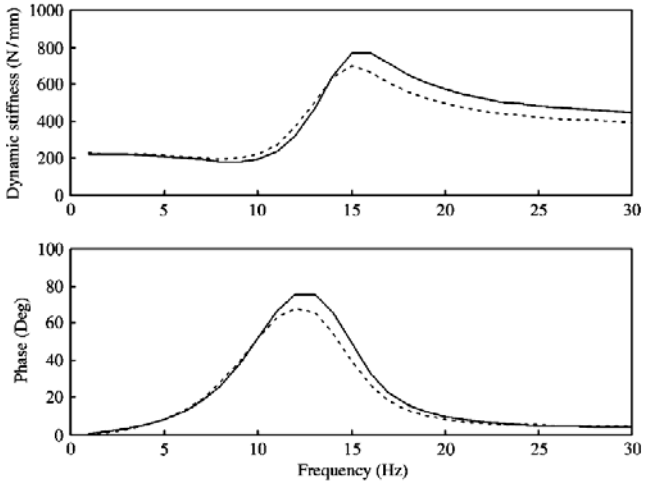

Fig. 22 Prediction using Model II over the lower frequency regime [12]. Key: — X = 2 mm; - - X = 1 mm.

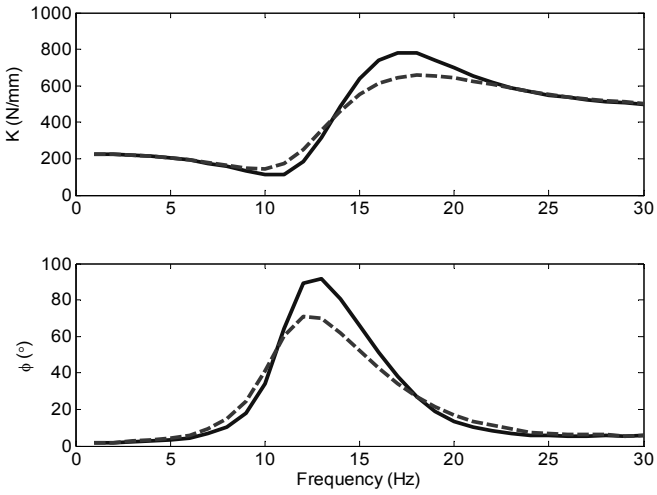

Fig. 23 Prediction using Model I over the lower frequency regime. Key: — X = 2 mm; - - X = 1 mm.

ACKNOWLEDGMENTS

We acknowledge the experimental efforts of J. Lopez Tellez (from General Motors) on mount G. Prior researchers whose models and data are evaluated here are also thanked for their pioneering work.

REFERENCES

1. R. Singh, G. Kim and P. V. Ravindra, “Linear analysis of automotive hydro-mechanical mount with emphasis on decoupler characteristics”, J. Sound Vib. 158, 219-243 (1992).
2. T. Ushijima, K. Takano and H. Kojima, “High performance hydraulic mount for improving vehicle noise and vibration”, SAE Paper 880073 (1988).
3. K. H. Lee and Y. T. Choi, “Performance analysis of hydraulic engine mount by using bond graph method”, SAE Paper 951347 (1995).
4. J. E. Colgate, C. T. Chang, Y. C. Chiou, W. K. Liu and L. M. Keer, “Modeling of a hydraulic engine mount focusing on response to sinusoidal and composite excitations”, J. Sound Vib. 184(3), 503-528 (1995).
5. A. Geisberger, A. Khajepour and F. Golnaraghi, “Modeling of a Hydraulic Mount with a New MDOF Decoupler Using Bond-graphs”, HKK Conference and Symposium, Systems Design Engineering, University of Waterloo, June 13-19 (1999).
6. A. Geisberger, A. Khajepour and F. Golnaraghi, “Nonlinear modeling and experimental verification of a MDOF hydraulic engine mount”, Control of Vib. Noise- New Millennium, ASME (2000).
7. M. Tiwari, H. Adiguna and R. Singh, “Experimental Characterization of a Nonlinear Hydraulic Engine Mount”, Noise Control Eng. J. 51(1), 36-49 (2003).
8. H. Adiguna, M. Tiwari and R. Singh, “Transient Response of a Hydraulic Engine Mount”, J. Sound Vib. 268, 217-248 (2003).
9. S. He and R. Singh, “Improved Estimation of Linear and Nonlinear Hydraulic Mount Models for Transient Responses”, SAE Paper 2005-01-2411 (2005).
10. J. H. Lee, M. S. Bae and K. J. Kim, “Limitations of Mechanical Model With Lumped Mass in Representing Dynamic Characteristics of Hydraulic Mount”, SAE Paper 2003-01-1466 (2003).
11. S. Kim and R. Singh, “Multi-Dimensional Characterization of Vibration Isolators over a Wide Range of Frequencies”, J. Sound Vib. 245(5), 877-913 (2001).
12. A. Geisberger, A. Khajepour and F. Golnaraghi, “Non-linear modeling of hydraulic mounts: theory and experiment”, J. Sound Vib. 249, 371-397 (2002).

CONTACT

Professor Rajendra Singh
Acoustics and Dynamics Laboratory
Center for Automotive Research
The Ohio State University
Email: singh.3@osu.edu
Phone 614-292-9044
Website: www.AutoNVH.org